Electrostatic Double Layer Force between Two Spherical Particles in a Straight Cylindrical Capillary: Finite Element Analysis

Prodip K. Das, Subir Bhattacharjee,* and Walied Moussa

Department of Mechanical Engineering, 4-9 Mechanical Engineering Building, University of Alberta, Edmonton, AB T6G 2G8, Canada

Received September 5, 2002. In Final Form: February 12, 2003

A numerical solution of the nonlinear Poisson−Boltzmann equation based on finite element approximation is developed to assess the interaction force between two identical spherical particles located inside a straight cylindrical capillary. The interaction forces for constant potential and constant charge particle surfaces are calculated for different surface potentials on the cylinder wall, various particle sizes, and different cylinder radii. The interaction force between the spheres was affected significantly by the proximity of the charged cylinder wall, particularly for constant surface potential particles. The influence of the cylinder wall on the particle−particle interaction force was most pronounced when the particle radius was comparable to the cylinder radius. The results suggest that when the cylinder and the particle surfaces are like-charged (bearing the same sign of the charge or surface potential), the electrostatic repulsion between the two spherical colloids is considerably suppressed. Conversely, the interparticle repulsion is more pronounced when the cylinder wall is oppositely charged with respect to the particles. The possibility of inducing a force modulation between two charged particles by altering the surface potential of the confining cylindrical wall appears to be viable on the basis of these simulations.

1. Introduction

Interaction between colloidal particles in confined domains is of great interest in a variety of applications involving colloidal and complex fluids, for instance, in capillary electrophoresis, chromatographic separations, transport of colloids through porous media, and membrane separations.[1,2] The Derjaguin−Landau−Verwey−Overbeek (DLVO) interaction potential[3,4] is usually at the core of most theories and mathematical treatments of such processes. The interaction between two colloidal particles in the framework of the DLVO theory is expressed as a sum of Lifshitz−van der Waals (LW) and electrostatic double layer (EDL) interactions.[5] Of these two interactions, the electrostatic double layer component is susceptible to immense variations with several operating and physicochemical conditions such as ionic strength of the suspending medium, the charging behavior of the interfaces, the dielectric property of the solvent, and geometry of the particles and the confining domain. Accordingly, the nature and magnitude of the electrostatic interactions are usually the primary governing parameters that dictate the overall macroscopic behavior of colloidal systems near interfaces and in confined domains.

Considerable attention has been devoted toward the calculation of the electrostatic double layer interaction between two colloidal particles in a confined domain over the past few years.[6−12] Most of these theoretical studies were spurred by the experiments that indicated the existence of a long-range attraction between the colloidal particles in a confined domain.[13] Although it has become increasingly apparent that the long-range attraction observed in these experiments could not be replicated in the framework of the Poisson−Boltzmann (PB) theory,[11,12] there still remains a scope of exploring the short-range electrostatic interaction between colloidal particles in a confined space in the framework of the PB equation.

A variety of numerical solution schemes for the Poisson−Boltzmann equation have been presented.[14−17] Most of these numerical studies primarily deal with the solution of the PB equation to obtain the interaction between two spherical colloidal particles or that between a particle and an infinite planar surface. These studies primarily rely on finite difference techniques and generally employ coordinate transformations to map the physical space into a rectangular computational grid. Application of the finite element technique or its generalizations is relatively less prevalent, and only recently several studies exploring the solution of the PB equation for different geometries using this technique have appeared in the literature.[12,18,19]

* Corresponding author. Tel: (780) 492 6712. Fax: (780) 492 2200. E-mail: subir.b@ualberta.ca.

(1) Masliyah, J. H. *Electrokinetic Transport Phenomena*; AOSTRA: Edmonton, Canada, 1994; Vol. 12.
(2) Elimelech, M.; Gregory, J.; Jia, X.; Williams, R. *Particle Deposition & Aggregation. Measurement, Modeling and Simulation*; Butterworth-Heinemann: Oxford, U.K., 1995.
(3) Derjaguin, B. V.; Landau, L. *Acta Physicochim.* (*URSS*) **1941**, *14*, 633.
(4) Verwey, E. J.; Overbeek, J. Th. G. *Theory of Stability of Lyophobic Colloids*; Elsevier: Amsterdam, 1948.
(5) Russel, W. B.; Saville, D. A.; Schowalter, W. R. *Colloidal Dispersions*; Cambridge University Press: Cambridge, 1989.
(6) Ospeck, M.; Fraden, S. *J. Chem. Phys.* **1998**, *109*, 9166.
(7) Bowen, W. R.; Sharif, A. O. *Nature* **1998**, *393*, 663.
(8) Bowen, W. R.; Sharif, A. O. *Nature* **1999**, *402*, 841.
(9) Bowen, W. R.; Williams, P. M. *Colloids Surf., A* **2002**, *204*, 103.
(10) Sader, J. E.; Chan, D. Y. C. *J. Colloid Interface Sci.* **1999**, *218*, 423.
(11) Sader, J. E.; Chan, D. Y. C. *Langmuir* **2000**, *16*, 324.
(12) Gray, J. J.; Chiang, B.; Bonnecaze, R. T. *Nature* **1999**, *402*, 750.
(13) Larsen, A. E.; Grier, D. G. *Nature* **1997**, *385*, 230.
(14) Glendinning, A. B.; Russel, W. B. *J. Colloid Interface Sci.* **1983**, *93*, 95.
(15) Carnie, S. L.; Chan, D. Y. C.; Stankovich, J. *J. Colloid Interface Sci.* **1994**, *165*, 116.
(16) Stankovich, J.; Carnie, S. L. *Langmuir* **1996**, *12*, 1453.
(17) Warszynski, P.; Adamczyk, Z. *J. Colloid Interface Sci.* **1997**, *187*, 283.
(18) Bowen, R. W.; Sharif, A. O. *J. Colloid Interface Sci.* **1997**, *187*, 363.
(19) Bowen, W. R.; Sharif, A. O. *J. Colloid Interface Sci.* **1997**, *188*, 517.

10.1021/la0207567 CCC: $25.00
Published on Web 04/15/2003

Predominantly, the problem addressed using this technique involves the evaluation of the electrostatic interaction force between two colloidal particles located on the axis of a cylindrical cavity. The finite element approach for obtaining the interaction force for this geometry, however, seems to have spurred a controversy following the numerical results shown by Bowen and Sharif.[7] In their study, it was reported that a long-range attraction would exist between the particles when these are confined in a cylindrical pore. This unusual result was almost immediately questioned by several authors, and it has been shown subsequently that the attractive force between two similarly charged colloidal particles in a cylindrical confinement is physically unrealistic in the framework of the PB equation.[9,11,12]

An inherent advantage of using the finite element technique for obtaining the interaction force between two particles in a cylindrical cavity is its ability to consider arbitrary geometrical domains. Furthermore, one can avoid coordinate transformations and directly apply the technique in a coordinate system that facilitates representation of the physical domain. The only problem with adoption of the finite element technique is perhaps the computational load it involves, specifically when stringent accuracy of the numerical results is warranted. However, several commercial finite element solvers of a general nature have become available recently and have substantially simplified the implementation of this technique to solve a variety of problems quite accurately. In this context, it is felt that if the accuracy and relevance of this technique can be demonstrated in solving the widely discussed problem of obtaining the interaction force between two particles in a charged cylindrical capillary, there might be greater interest in exploring finite element based solutions of the PB equation for several geometries of practical concern.

In this study, we present a numerical solution of the nonlinear Poisson−Boltzmann equation based on finite element analysis to evaluate the net interaction force between two spherical colloidal particles confined in a cylindrical capillary. The interaction force is computed for different surface potentials on the wall of the cylindrical enclosure. Through several simulations encompassing wide ranges of the parameters governing the electrostatic interaction, we explore the conditions under which the presence of the cylindrical wall modifies the electrostatic force between the spherical particles substantially from the corresponding force between the two particles in an infinite medium.

2. Electrostatic Interaction between Spherical Particles in a Cylindrical Capillary

In this section, we present the general statement of the electrostatic problem in terms of the nonlinear Poisson−Boltzmann equation and express this equation and the pertinent boundary conditions for a cylindrical domain containing two spherical colloidal particles. The formal description of the governing equations and boundary conditions is presented, accompanied by an outline of the procedure of scaling the governing equations.

2.1. Nonlinear Poisson−Boltzmann Equation. The nonlinear PB equation can be written for a symmetric (ν:ν) electrolyte as

$$\nabla^2\Psi = \kappa^2 \sinh(\Psi) \tag{1}$$

Here Ψ ($=\nu e\psi/kT$) is the scaled potential, ν is the charge number of the ions, e is the magnitude of electronic charge, ψ is the electrostatic potential expressed in volts, k is the Boltzmann constant, and T is the absolute temperature. The parameter κ is the inverse Debye screening length, defined as

$$\kappa = \sqrt{\frac{2n_\infty e^2\nu^2}{\epsilon\epsilon_0 kT}} \tag{2}$$

where n_∞ is the bulk concentration of the ions (in numbers/m^3), ϵ is the dielectric constant of the suspending fluid, and ϵ_0 is the dielectric permittivity of a vacuum.

In this study, it is assumed that the particles and the cylinder are perfect dielectrics ($\epsilon = 0$), and hence, we will only solve the PB equation in the electrolyte medium (the so-called outer problem). Although it is straightforward to consider finite dielectric constants for the materials constituting the particles and the confining walls of the domain, and although such an approach will lead to a more rigorous analysis of the electrostatic problem, we resort to solving the outer problem to conform to earlier studies against which we compare our results for some limiting cases.[15,16]

Depending on the charging behavior of the surfaces immersed in the dielectric, the electrostatic interaction may be calculated assuming constant surface potential, constant surface charge, or surface charge regulation boundary conditions at the solid−liquid interfaces.[11,15,20] Usually, most charged interfaces in aqueous electrolyte media tend to obey some form of a charge regulatory behavior. However, it is known that constant potential (CP) and constant charge (CC) conditions represent the limiting charging behaviors of the interfaces and provide a lower and an upper bound of the interaction, respectively.[15] Accordingly, in the present investigation, we consider both CP and CC cases to obtain the lower and upper bounds of interaction between two charged particles. The constant potential boundary condition is represented as

$$\Psi = \Psi_p \qquad \text{for } \partial\Omega \in \text{solid−liquid interface} \tag{3}$$

where Ψ_p is the surface potential of the solid−liquid interface, and $\partial\Omega$ represents the boundary of the computational domain. The constant charge boundary condition can be represented as

$$-\mathbf{n}\cdot\nabla\Psi = \sigma_p \qquad \text{for } \partial\Omega \in \text{solid−liquid interface} \tag{4}$$

where $\mathbf{n}$ is the unit normal to the solid−liquid interface pointing to the electrolyte, and σ_p is the scaled surface charge density, related to the interfacial charge density q_p (C/m^2) as

$$\sigma_p = \frac{\nu e q_p}{\kappa\epsilon\epsilon_0 kT} \tag{5}$$

Thus, known values of the surface potential Ψ_p or the surface charge density q_p provide the necessary boundary conditions at the solid−liquid interfaces.

The above equations provide the generalized formulation of the electrostatic problem. Solution of the PB equation in a given geometrical framework requires recasting eq 1 in the proper coordinate system representing the geometry and defining the boundary conditions at all the solid−liquid interfaces. In the following, we set up the governing equations leading toward the calculation of elec-

(20) Carnie, S. L.; Chan, D. Y. C. *J. Colloid Interface Sci.* **1993**, *155*, 297.

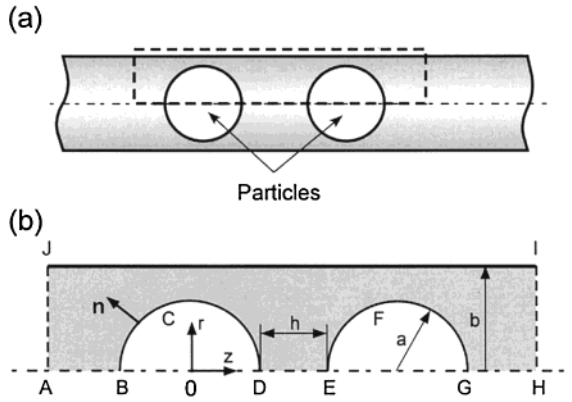

Figure 1. Schematic depiction of two spherical colloidal particles inside a cylindrical capillary (a). The particle centers are located on the cylinder axis. The region circumscribed by the broken lines depicts the computational domain, shown in detail in part b. Utilizing the symmetry around the horizontal axis, the two-dimensional formulation of the governing equation was developed. The arcs BCD and EFG represent the particle surfaces, while the line IJ represents the wall of the cylindrical capillary. The origin of the cylindrical coordinate system is located at O.

trostatic force on a particle in a system comprising two colloidal particles within a charged cylindrical capillary.

2.2. Computational Geometry and Boundary Conditions. Figure 1 shows the geometry under consideration in the present investigation along with the coordinate framework. Here, two spherical colloidal particles of radius a are separated by a distance h (distance of closest approach) in an infinitely long straight cylindrical capillary of radius b. The particle surfaces are treated as either constant surface potential or constant surface charge density boundaries. The computational domain used in the finite element modeling is depicted by the rectangular region (in dashed lines) in Figure 1a. The particle centers lie on the axis of the cylindrical capillary, rendering the problem to be axisymmetric in a cylindrical coordinate system. Figure 1b shows the geometric details of the computational domain. The surfaces of the two particles (arcs BCD and EFG) are assigned constant surface potentials ψ_p or constant charge densities q_p in different simulations. The wall of the cylinder (solid line IJ) is assigned a constant surface potential ψ_c. On the remaining parts of the boundary, we apply appropriate symmetry boundary conditions. The cylindrical coordinate system is chosen such that the center of the particle BCD is located at the origin.

In the cylindrical coordinate system, the PB equation (eq 1) is written as

$$\frac{\partial^2\Psi}{\partial r^2} + \frac{\partial^2\Psi}{\partial z^2} = \kappa^2 \sinh(\Psi) - \frac{1}{r}\frac{\partial\Psi}{\partial r} \tag{6}$$

by noting that the potential is independent of the angular coordinate θ. As mentioned earlier, we solve this equation only in the electrolyte solution, shown by the shaded region in Figure 1b. The boundary conditions for constant surface potential on the spheres and the cylinder are

$$\Psi = \Psi_p \quad \text{for } \partial\Omega \in \text{BCD and EFG} \tag{7a}$$

$$\Psi = \Psi_c \quad \text{for } \partial\Omega \in \text{IJ} \tag{7b}$$

$$\mathbf{n}\cdot\nabla\Psi = 0 \quad \text{for } \partial\Omega \in \text{AB, DE, GH, HI, and JA} \tag{7c}$$

The last statement, eq 7c, provides the symmetry conditions on the fluid boundaries, implying that the potential gradients normal to these line segments are zero. In this equation, **n** represents the unit normal to the surface. Clearly, this is an artificial boundary condition on the segments JA and HI, and appropriate measures must be taken in the numerical solution to ensure that this artificial boundary condition does not influence the accuracy of the solution.

For constant charge particles, the appropriate boundary condition is

$$-\mathbf{n}\cdot\nabla\Psi = \sigma_p \quad \text{for } \partial\Omega \in \text{BCD and EFG} \tag{8}$$

with the other boundary conditions, eqs 7b and 7c, remaining the same as in the constant potential case.

The surface charge density of an isolated charged sphere is related to the surface potential through[5]

$$q_p = \frac{Q_p}{4\pi a^2} = \frac{\epsilon\epsilon_0 kT}{e\nu}\kappa\left[2\sinh\left(\frac{1}{2}\Psi_{p,\infty}\right) + \frac{4}{\kappa a}\tanh\left(\frac{1}{4}\Psi_{p,\infty}\right)\right] \tag{9}$$

where q_p is the surface charge density (C/m^2), Q_p is the total surface charge, and $\Psi_{p,\infty}$ is the surface potential of an isolated spherical particle. Introducing the scaled charge density, eq 5, we get

$$\sigma_p = 2\sinh\left(\frac{1}{2}\Psi_{p,\infty}\right) + \frac{4}{\kappa a}\tanh\left(\frac{1}{4}\Psi_{p,\infty}\right) \tag{10}$$

We employ this relationship to define the charge density based on a given surface potential on the spherical particles in isolation. The semiempirical relationship, eq 9, is known to provide the charge density to within 5% of the exact charge density on an isolated sphere for $\kappa a > 0.5$.[5]

2.3. Calculation of Electrostatic Force. Once the potential distribution is obtained by solving the PB equation, the electrostatic force on any one of the spherical particles can be calculated by integrating the total stress tensor, defined as

$$\mathbf{T}_{ij} = \left(\Pi - \frac{1}{2}\epsilon\epsilon_0\mathbf{E}\cdot\mathbf{E}\right)\mathbf{I} + \epsilon\epsilon_0\mathbf{E}\mathbf{E} \tag{11}$$

over the surface of the particle, yielding

$$\mathbf{F} = \int_p\int \mathbf{T}_{ij}\cdot\mathbf{n}\,dS = \int_p\int \left[\left(\Pi - \frac{1}{2}\epsilon\epsilon_0\mathbf{E}\cdot\mathbf{E}\right)\mathbf{I} + \epsilon\epsilon_0\mathbf{E}\mathbf{E}\right]\cdot\mathbf{n}\,dS \tag{12}$$

where the subscript p represents integration over the closed particle surface. Here, **F** is the force acting on the sphere, **E** ($=-\nabla\psi$) is the electrostatic field vector, Π is the osmotic stress, **n** is the unit surface normal (Figure 1b), and **I** is the identity tensor. The above expression of force is independent of the choice of the surface over which the integration is performed. It can be performed on the closed surface of any of the particles or at the midplane of these particles. In the present investigation, the net stress tensor is integrated over the surface of a particle to calculate the net force on the particle.

The net force acting on a sphere along the axial (z) direction can determined from the total force **F** and can be written explicitly as

$$F_z = \mathbf{F}\cdot\mathbf{k} = 2\pi\kappa^2\epsilon\epsilon_0\left(\frac{kT}{\nu e}\right)^2\int_{BCD}\left[n_r\left\{(\cosh\Psi - 1) + \frac{1}{2}(\Psi_z^2 - \Psi_r^2)\right\} + n_z\Psi_r\Psi_z\right]r\,dr \tag{13}$$

where **k** is a unit vector in the positive z direction, n_r and n_z are the components of the unit normal along the r and z directions, respectively, and BCD represents the semicircular boundary of the spherical particle over which the integration is performed. Ψ_r and Ψ_z are the components of the electric field vector **E** along the r and z directions, respectively. The term $(\cosh \Psi - 1)$ in eq 13 represents the osmotic pressure contribution to the net force, while the two remaining terms in the square brackets represent the electrostatic (Maxwell) stress. Since the integral of the osmotic pressure term vanishes over a closed domain having a constant potential, the force for CP situations is calculated by excluding the osmotic pressure term from eq 13. For CC cases, both the osmotic and electrostatic stresses are included in the force expression. The axial force (the force along the z-direction) is represented in its nondimensional form as

$$f_z = \frac{F_z}{\epsilon\epsilon_0}\left(\frac{\nu e}{kT}\right)^2 \tag{14}$$

in the rest of this paper.

3. Numerical Solution Using the Finite Element Technique

The numerical solution of the PB equation was performed using finite element analysis. Details regarding implementation of finite element approximation to solve partial differential equations (PDEs) are available in standard textbooks.[21] Our goal was to employ a generalized technique that is widely available and can be implemented relatively easily on most commercial finite element software. Consequently, in this section, we have only focused on the details of the procedure followed to formulate the problem, the types of elements used, and the methodology of adaptive mesh refinement and error control. The formulation of the problem, specifically the statement of the problem in a generalized PDE form, and subsequent recasting in the weak form were crucial for a successful and fast solution. Furthermore, the adaptive mesh refinement steps and refinement criteria stated here provided the fastest and accurate convergence of the solution.

3.1. Weak Form of the PB Equation. The governing PB equation (eq 6) is rendered nondimensional by scaling the radial and axial coordinates with respect to the Debye screening length, yielding the following form

$$\frac{\partial^2\Psi}{\partial\bar{r}^2} + \frac{\partial^2\Psi}{\partial\bar{z}^2} = \sinh(\Psi) - \frac{1}{\bar{r}}\frac{\partial\Psi}{\partial\bar{r}} \tag{15}$$

in terms of the scaled variables $\bar{r} = \kappa r$ and $\bar{z} = \kappa z$. We note that this equation represents a general PDE formulation of the type

$$\bar{\nabla}\cdot\Gamma = \mathbf{R} \tag{16}$$

where $\Gamma = \Psi_{\bar{r}} + \Psi_{\bar{z}}$, with the subscripts representing the partial derivatives with respect to $\bar{r}$ and $\bar{z}$, and

$$\mathbf{R} = \sinh(\Psi) - \frac{1}{\bar{r}}\frac{\partial\Psi}{\partial\bar{r}} \tag{17}$$

To implement a finite element solution, the governing PDE is rewritten in its weak form, which is obtained by writing eq 16 as an equality of the integrals[22]

$$\int_\Omega v\nabla\cdot\Gamma \, dA = \int_\Omega v\mathbf{R} \, dA \tag{18}$$

where v is a test function. Applying Green's theorem, the area integral in the left-hand side of the above equation can be written as a line integral over the domain boundary. Furthermore, applying a Neumann boundary condition,

$$-\mathbf{n}\cdot\Gamma = \mathbf{G} \qquad \text{on } \partial\Omega \tag{19}$$

the weak formulation of the governing PDE is given as

$$\int_\Omega(\nabla v\cdot\Gamma + v\mathbf{R}) \, dA + \int_{\partial\Omega} v\mathbf{G} \, ds = 0 \tag{20}$$

Here the function **G** defines the generalized Neumann boundary coefficient. The term ds in the final integral represents a small length element on the domain boundary. The weak problem can be further constrained through a Dirichlet boundary condition, stated as

$$\mathbf{Q} = 0 \qquad \text{on } \partial\Omega \tag{21}$$

where **Q** represents a vector of Dirichlet boundary conditions.

Equations 20 and 21 constitute the weak form of the governing PDE that can be solved using the finite element technique.

3.2. Numerical Solution Procedure. The computational domain was initially discretized into a triangular mesh, and Lagrangian elements of second order (quadratic elements) were used. The use of the quadratic elements implies that we have six nodes on a triangular element (three at the vertexes and three at the midpoints of each side). For each of these nodes, we have a shape function φ_i with U_i degrees of freedom. The shape functions are quadratic polynomials with $\varphi_i = 1$ at node i, and $\varphi_i = 0$ at all other nodes. In terms of the basis functions and degrees of freedom, the solution can be written for an element as

$$\Psi = \sum_i U_i\varphi_i \tag{22}$$

where the summation is over all the nodes in the element. The weak form of the governing PDE was discretized by assuming the test function v to be the shape function φ_i in each element.

A nonuniform initial mesh was generated in each simulation using triangulation of the domain. The mesh was created to ensure that the domain error was small at the curved surfaces of the sphere, yielding smaller elements near the circular boundaries in Figure 1b. The solution of the final assembled matrix equation was achieved by Gauss elimination. After solution, the local error in each element was calculated either by using a linear functional estimator or by computing an L^2 norm of the error. This error was then used to refine the mesh. The mesh refinement was usually performed on all the elements where the error estimate was larger than the preset tolerance (10^{-6}). The mesh refinement was achieved by dividing each original element into four elements. The refinement technique ensured that all hanging nodes were removed from the mesh. It was also ensured that none of the refined elements had vertexes smaller than half the vertexes of the original elements.

(21) Zienkiewicz, O. C.; Taylor, R. L. *The Finite Element Method*, 5th ed.; McGraw-Hill: New York, 1989.

(22) Reddy, J. N. *An Introduction to the Finite Element Method*, 2nd ed.; McGraw-Hill: New York, 1993.

The process of obtaining a solution, determination of the local error in each element, and mesh refinement was repeated until a global convergence criterion was attained. We also imposed limits on the maximum number of iterations in mesh refinement (10) and the maximum number of elements (20 000). The program was terminated when any of the abovementioned criteria was attained. After termination, the postprocessing of the data involved calculation of the interaction force on the boundaries of the spherical particles. A four-point Gaussian quadrature was used to compute the force. We computed the force on both the sphere surfaces and compared these values. In all the reported results, the forces obtained on the two sphere surfaces match to within two significant digits. As mentioned in section 2.2, the boundary conditions on segments JA and HI (Figure 1b) are artificial symmetry conditions, which may be valid only when these boundaries are located sufficiently far away from the spheres. To ascertain the minimum distance between the sphere surface and the domain boundary (length of the segments AB and GH) that would lead to negligible error in the computed forces, the simulations were performed by setting this distance (AB or GH) to different values ranging from κa to $10\kappa a$. The resulting force computations indicated that the influence of this artificial boundary becomes negligible when the lengths of the segments AB and GH are set to values of $\geq 2\kappa a$.

The entire solution methodology was developed using a commercially available software FEMLAB (COMSOL Inc., USA), which can be run either as a programmable toolbox for development of finite element solutions on MATLAB (The MathWorks, Inc., USA) or as a simple graphical user interface (GUI) based integrated environment for solution of partial differential equations using the finite element technique. It was observed that considerable programming flexibility could be achieved by using a sequence of function or procedural calls to various subroutines from the FEMLAB toolbox for implementing the various steps of the finite element procedure, while relegating all the peripheral calculations to MATLAB. All the calculations were performed on a Pentium III (1000 MHz) personal computer.

4. Results and Discussion

In this section, we first focus on the accuracy of the finite element calculations for the limiting case of two identical charged spheres in an infinite electrolyte medium. This is achieved by comparing the presently obtained force estimates with those available in other reported works. Following this, the interaction force between two spheres in a cylindrical capillary is obtained for various combinations of the governing parameters to highlight the dependence of this force on the proximity of the charged cylinder wall.

4.1. Interaction between Two Charged Spherical Particles. In this subsection, results are shown for one of the limiting cases of the model, namely, interaction between two identical spherical particles in an infinite domain. The simulation results presented here are obtained for both the CP and CC conditions on the particle surfaces. These numerical solutions were obtained by assuming the cylinder radius b to be considerably larger than the particle radius a. A value of 0.2 for the parameter $\lambda = a/b$ (size ratio) was used to ensure that the influence of the cylindrical domain on the sphere−sphere interaction would be minimal. Furthermore, a Neumann boundary condition was applied on the cylinder wall (IJ in Figure 1b):

$$\mathbf{n}\cdot\nabla\Psi = 0 \qquad \text{on IJ} \tag{23}$$

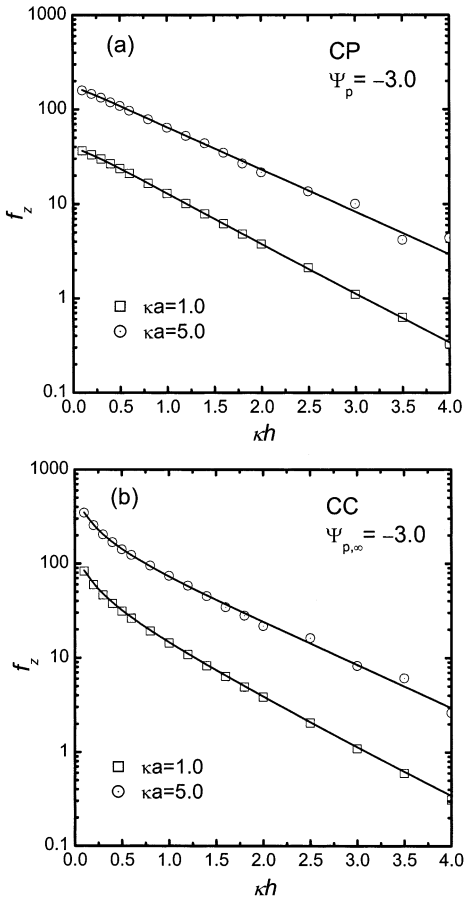

Figure 2. Variation of the electrostatic interaction force between two identical charged particles in an unbounded electrolyte with scaled separation distance, κh, corresponding to two values of scaled particle size, κa, for (a) constant potential (CP) and (b) constant charge (CC) conditions. Solid lines represent the results from an independent numerical result based on a Hermite collocation technique in a bispherical coordinate system (see text). Symbols represent the finite element results obtained in the present work. The charge density used in the CC calculations was based on a scaled surface potential of −3.0 on the isolated particles. In the finite element solutions, it was obtained by employing eq 9, while in the collocation method it was obtained by numerically solving the PB equation around an isolated sphere.

Using these conditions, the interaction force between the two spheres was computed without modifying the problem geometry or the coordinate system. The objective of employing this approach was to observe the influence of the cylindrical coordinate system on the error in force calculations. The cylindrical coordinate system has rarely been used for studying the interaction force between two spherical colloids. Typically, numerical solution of this problem is achieved by using a bispherical coordinate system, which maps the spherical physical domain to a rectangular computational domain.[15,17] Furthermore, the use of bispherical coordinates maps the infinite domain problem onto a finite grid, allowing one to use the more accurate boundary condition $\Psi = 0$ at ∞. It has generally been speculated that solution of the PB equation in other types of coordinate frameworks might lead to erroneous estimates of the interaction force for the two-sphere problem discussed here.

Figure 2 depicts a comparison of the interaction forces obtained in the present study (symbols) with the corresponding numerical estimates obtained through the solution of the PB equation in a bispherical coordinate system (solid lines). The solution in the bispherical

coordinate system was obtained using a cubic Hermite collocation based discretization scheme, followed by iterative solution of the resulting nonlinear system of equations by a Newton−Raphson technique.[15,16] The interaction forces obtained under both CP and CC conditions using the two techniques are virtually identical over a relatively wide range of scaled surface-to-surface separation distances $0 < \kappa h < 3$. The finite element solution becomes unreliable at larger separations, particularly for the larger value of the parameter κa. While the finite element estimates start to deviate from the collocation results beyond scaled separation distances of 3 for $\kappa a = 5$, the two estimates of the interaction force are in excellent agreement up to separation distances of 4 for $\kappa a = 1$. Although higher accuracy can be achieved at greater separations by further mesh refinement, this was deemed as an enormous computational effort to obtain a relatively insignificant electrostatic force. The scaled forces at small separations ($\kappa h < 2$) obtained from the two techniques were within 3% for both values of κa for the CP condition and within 5% for the CC condition. In general, for a given number of elements and accuracy settings, the forces estimated under the CP condition tend to be more accurate than the CC results.

The comparison of the presently obtained finite element estimates of the force with an independent numerical result based on a completely different technique highlights several points worth noting about the nature of finite element solutions of the nonlinear PB equation. Three key differences in the two solution techniques can be readily identified: (i) The present results were obtained in a cylindrical coordinate system, whereas the collocation technique used a bispherical coordinate system. (ii) The boundary condition representing the cylindrical wall was chosen to be of the Neumann type, which may be construed as an artificial boundary condition to the PB equation, while the boundary condition used in the bispherical coordinate system is the true condition ($\Psi = 0$) at infinite separation. (iii) The integral for force calculation was evaluated on the sphere surface in the finite element calculation, while the integral was preferably performed over the midplane between the spherical particles in the collocation method noting that the integration over the particle surface results in relatively larger errors. Despite these differences, the two techniques provide almost identical results at small particle−particle separations.

Although the comparison of the two results indicates the ability of finite element approximations to provide a reasonable estimate of the interaction forces, particularly at small values of particle−particle separations, it comes at the expense of fairly involved computation. The results in Figure 2 could not be attained without (a) using adaptive meshing, (b) using a large number of elements (usually of the order of 20 000), and (c) carefully choosing the convergence criterion. Furthermore, the governing equation had to be stated in a very specific manner to achieve the given accuracy. These might be an artifact of our usage of a general-purpose commercial software for the computation, which may not be specialized for solution of the PB equation. We used almost all of the standard features enabling high-accuracy solutions, such as adaptive solvers, multiple criteria for error minimization, and mesh adaptation. Yet, with none of the available combinations could a convergence of the force to within a given tolerance be obtained by using fewer elements. However, in terms of accuracy, the finite element solutions for this limiting case are the worst compared to any of our subsequent calculations. This is due to the following reasons: (a) the computational domain used in these calculations was the largest to ensure that the artificial boundary effects were negligible on the solution; (b) most of the boundary conditions used (except for the ones on the particle surfaces) were artificial; and (c) in the CC results, there may be an error (≤5%) in the estimates of the surface charge density calculated using eq 9 compared to the values obtained using the numerical solution of the nonlinear PB equation around a single sphere.[5]

Clearly, the solution of the PB equation for two spherical particles could have been more facile if the coordinate system of the problem was bispherical, rendering the computational grid to be rectangular. However, this option was ruled out because the primary objective of this study was to obtain the interaction force between the two spherical particles in a confined cylindrical domain, for which the present coordinate system seems natural and allows us to reduce the dimensionality of the problem by utilizing axisymmetry.

4.2. Particles in a Capillary: Like-Charge Interaction Forces. The interaction forces between two spherical particles located on the axis of a charged cylindrical capillary were obtained for CP and CC boundary conditions on the spheres. The force was determined for wide ranges of the scaled particle size κa and the size ratio λ (=a/b) and for different combinations of the surface potentials on the particles and the cylinder wall. In the following, we depict some of the key simulation results highlighting the influence of the pore wall on the particle−particle interaction force.

Figure 3 shows the variation of the scaled interaction force with scaled separation distance between the particles (κh) under CP conditions on both the spheres and the cylinder wall. The results in Figure 3a−d correspond to four values of the scaled particle size (κa), namely, 0.5, 1.0, 2.0, and 5.0, respectively. In all these figures, the force is calculated for a fixed value of the size ratio $\lambda = a/b = 0.83$ and a fixed dimensionless surface potential $\Psi_p = -3$ on the particles. For comparison, the interaction force between two spheres in an infinite electrolyte is depicted as open symbols in Figure 3b,d corresponding to $\kappa a = 1$ and $\kappa a = 5$, respectively. These figures indicate that varying the dimensionless cylinder surface potential (Ψ_c) from 0 to −5 induces a dramatic lowering of the magnitudes of the electrostatic force, particularly for small values of $\kappa a \leq 2$. For larger values of κa, the interaction force between the particles is not seriously affected by the charge on the cylinder wall. For small κa (for instance, $\kappa a = 1$), we observe a deviation of the interaction force between the confined spheres from the corresponding force between these spheres in an infinite medium even when the cylinder wall bears no charge (Figure 3b, solid line and symbols).

An important observation from these results is that all of the force profiles remain in the positive quadrant, indicating that the force never changes sign over the scaled separation distances shown ($0 < \kappa h < 3$). These results corroborate the fact that it is theoretically impossible to obtain electrostatic attraction between two constant potential spherical particles (with same surface potentials) even in charged confined domains.[11] We note that these results were obtained for a considerably large value of the size ratio compared to the calculations of Bowen and Sharif.[7] Our results also show the same qualitative trends observed by Gray et al.[12] when the particle to cylinder size ratio λ is large.

The forces corresponding to CC conditions on the sphere surfaces are shown in Figure 4, which indicates a different behavior compared to the CP cases. These results were obtained under identical parameter settings for the CP

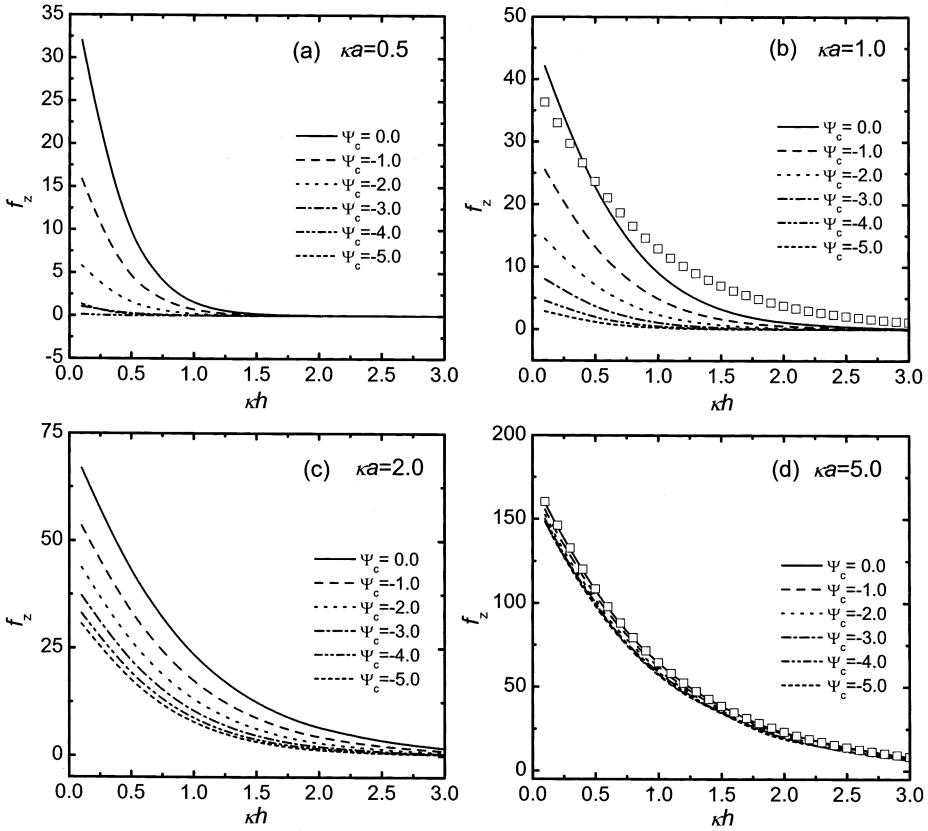

Figure 3. Electrostatic interaction force between two particles in a cylindrical capillary corresponding to different cylinder surface potentials. The variations of the scaled electrostatic force with scaled separation between the particles are depicted for a fixed size ratio (λ) of 0.83 and a fixed surface potential, $\Psi_p = -3.0$, on the particles (assuming constant potential particles). Different line types correspond to different surface potentials on the cylinder wall as indicated in the legend. The simulations were performed for four scaled particle sizes, indicated by the four values of κa in parts a−d. The open symbols in parts b and d depict the interaction force between two CP spheres in an unbounded electrolyte corresponding to the κa values shown in the legends.

simulations. The cylinder wall was assumed to behave as a CP surface in these calculations. It can be seen that the interaction forces for the CC case do not change as dramatically as the corresponding forces for the CP case when the cylinder surface potential is altered. The particle−particle interaction force decays more rapidly for larger cylinder surface potentials. The influence of the cylinder potential on the interaction force is not perceptible for $\kappa a = 5$ (Figure 4d). Once again, for all combinations of the governing parameters, we observe that the force remains repulsive over the entire range of particle−particle separations studied. Furthermore, for $\kappa a = 1$, the mere presence of an uncharged confining wall alters the magnitude of the electrostatic repulsion between the spheres, as seen previously in the CP case (Figure 4b, solid line and symbols).

4.3. Influence of Proximity of the Charged Wall. As observed in Figures 3 and 4, which depict the results for $\lambda = 0.83$, the interaction force between the two spheres is influenced by the proximity of the charged wall of the confining domain. Figure 5 depicts the extent to which the scaled force between two particles at a fixed separation distance $\kappa h = 0.4$ is affected by changes in the size ratio λ for different surface potentials on the cylinder wall. All the results were obtained for $\kappa a = 1$ and $\Psi_p = -3$, assuming CP boundary conditions on the particles. For fixed surface potentials on the cylinder, the interaction force decreases considerably with increasing values of λ. It is discernible that for small values of λ (when the particles are much smaller than the cylinder radius), the influence of the cylinder surface on the interaction between the particles will be minimal. Accordingly, the interaction force approaches the limiting value of the corresponding force between two spheres in an infinite domain as $\lambda \rightarrow 0$, irrespective of the magnitude of the cylinder surface potential. The case where the surface potential on the cylinder is zero (uppermost curve in Figure 5) indicates that the proximity of the cylinder wall has very little influence on the interaction force between the two spheres when it is uncharged.

A similar trend is observed for CC particles, as depicted in Figure 6. Here, the change in interaction force induced by variations in λ is more modest compared to the CP results. All the calculations were performed by keeping the simulation parameters the same as in Figure 5, except for the constant charge boundary condition on the particle surfaces. We observe the limiting behavior of the interaction force approaching the value of the force between two constant charge particles in an infinite medium as $\lambda \rightarrow 0$. The influence of the uncharged cylinder wall ($\Psi_c = 0$) on the particle−particle interaction force is manifested differently compared to the CP case, indicating a much larger influence of the cylinder wall on the interaction force between CC particles as it approaches closer to the interacting particles ($\lambda \geq 0.6$).

An interesting feature in the results corresponding to $\Psi_c = 0$ for the constant potential particles (Figure 5, uppermost curve) is the presence of a slight maximum near $\lambda = 0.7$. Although the variation of the interaction force between the particles with λ is quite small when the cylinder potential is zero, this behavior evolves from the variations in the electric field distribution around a given sphere due to the combined influence of the second particle and the proximity of the cylinder wall. When the cylinder

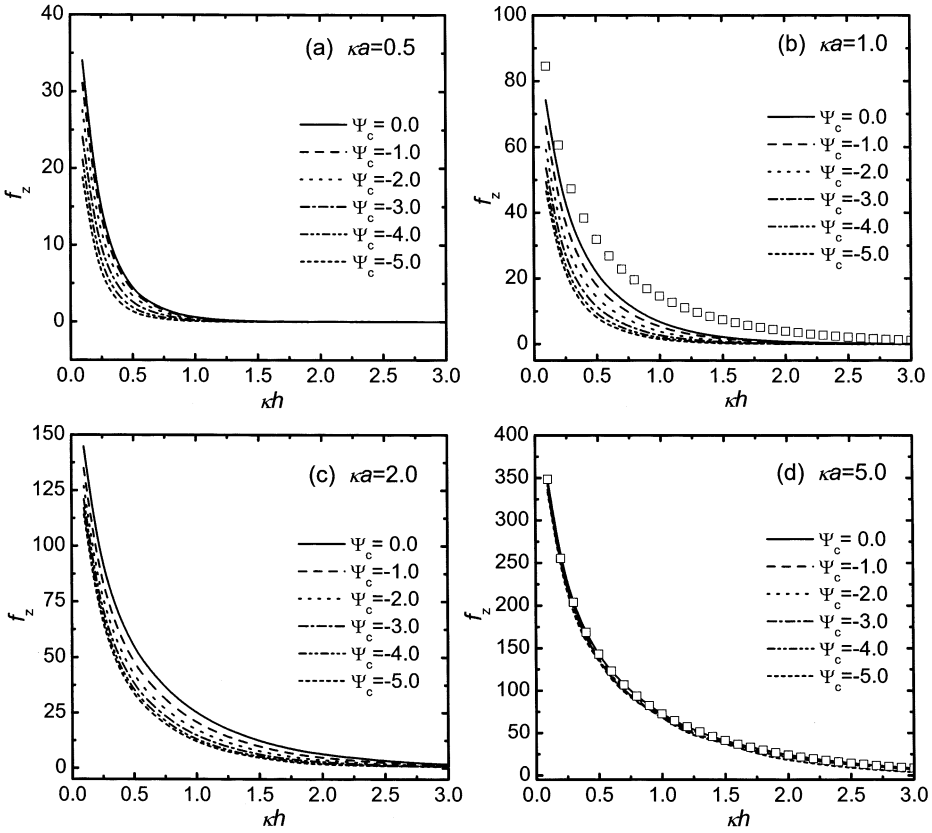

Figure 4. Variation of the scaled interaction force between two constant charge particles under same conditions as in Figure 3. The charge density on the spheres was evaluated assuming a surface potential $\Psi_{p,\infty} = -3.0$ on each particle at isolation.

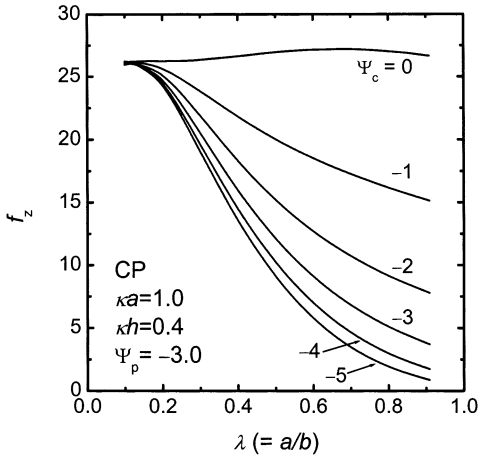

Figure 5. Dependence of the particle−particle interaction force on proximity of the charged cylinder wall. The dependence of the scaled interaction force between two constant potential particles on the size ratio λ is shown for several values of the cylinder surface potential.

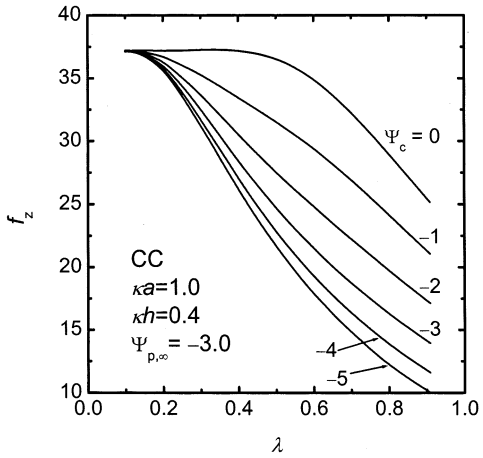

Figure 6. Dependence of the scaled particle−particle interaction force on λ for constant charge particles. Except for the CC boundary condition on the spheres, all other parameters are the same as in Figure 5.

wall is far from the particle surface, the electric field around a given sphere is primarily influenced by the second particle. As the cylinder radius becomes comparable to the particle radius, it starts to influence the potential distribution around the sphere. The maximum interaction force was observed when the particle−particle and the particle−cylinder separation distances were equal, that is, $\kappa h = \kappa(b - a)$. As the cylinder wall approached closer to the sphere compared to the other particle, the force was primarily governed by the influence of the cylinder wall. The maximum was not observed for the CC boundary conditions (Figure 6).

4.4. Modulation of Repulsion between Two Particles. Figure 7 shows the variation of the interaction force with scaled separation between the particles for four values of the size ratio. Two sets of results are shown, those corresponding to $\Psi_c = -3$ in Figure 7a and those corresponding to $\Psi_c = 0$ in Figure 7b. The other conditions were $\Psi_p = -3$, $\kappa a = 1.0$, and CP boundaries on the particles and the cylinder. For reference, the interaction force between two spheres in an infinite medium is shown as solid lines in Figure 7a,b. The interaction forces for small values of λ (upright and inverted triangles in Figure 7a) nearly coincide with the solid lines, indicating very little influence of the charged cylinder wall on the particle−

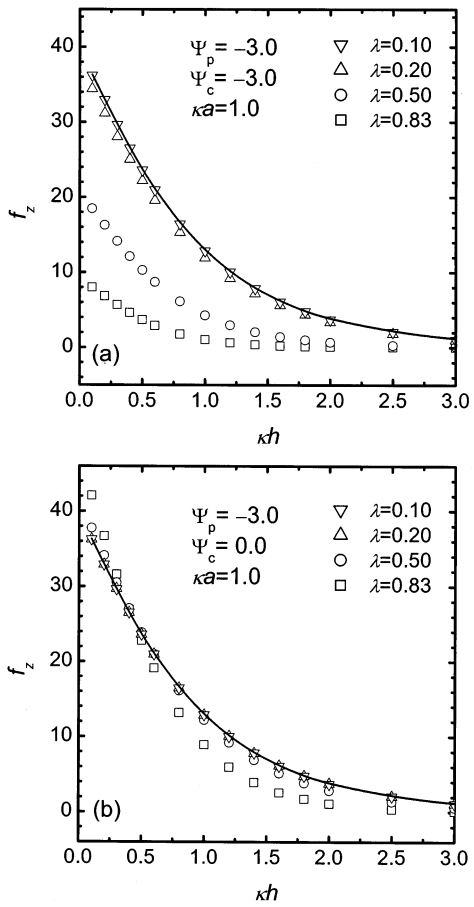

Figure 7. Interaction force at different scaled separations between CP particles corresponding to two values of the scaled cylinder surface potential: (a) $\Psi_c = -3$ and (b) $\Psi_c = 0$. The solid line depicts the interaction force between two spheres in an unbounded electrolyte. The different symbols correspond to different size ratios.

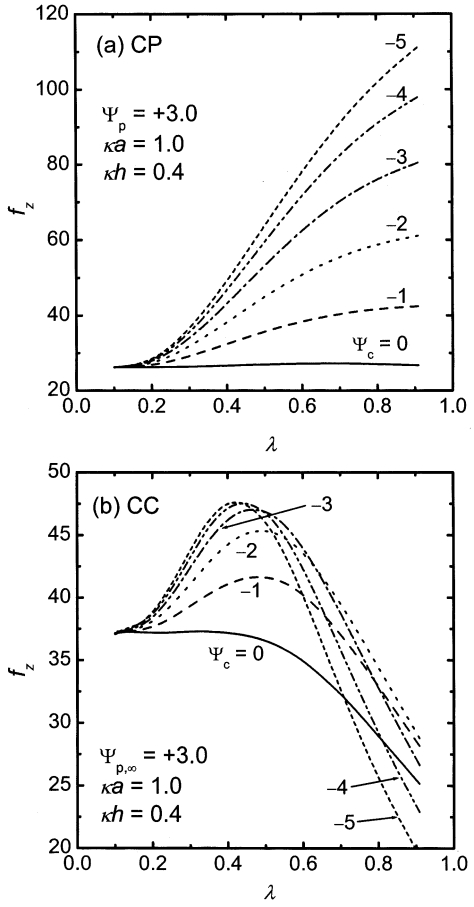

Figure 8. Interaction force between two identically charged spheres inside an oppositely charged capillary. The variation of the force with size ratio is shown for different cylinder surface potentials. Part a depicts the scaled interaction force for constant potential particles, while part b shows the scaled interaction force for constant charge particles.

particle interaction. As the extent of confinement increases (λ becomes larger), the force between the particles decreases considerably. The corresponding result for the case when the cylinder surface potential is zero (Figure 7b) depicts minor variations in the decay behavior of the interaction force for the four values of λ, the deviation from the limiting case of two spheres in an infinite medium increasing for larger λ. In fact, at small separations, $\kappa h < 0.4$, the interaction force between two spheres is greater than the corresponding force between the spheres in an infinite medium, although the variation is not quite significant. Hence, when the cylinder potential is zero, it may be assumed that the interaction force between the particles does not undergo a serious alteration with changes in the size ratio.

The large difference in the interaction forces between the particles corresponding to the cases when the cylinder surface potential has a finite value (On) and is zero (Off), depicted in Figure 7a,b, respectively, may be utilized as a control mechanism for the short-range ($\kappa h < 1$) colloidal forces between the particles. For instance, alternating the scaled surface potential of the cylinder between zero and -3 while keeping the particle separation fixed at $\kappa h = 0.4$ can induce an almost 1 order of magnitude change in the electrostatic interaction force for $\lambda = 0.83$ (Figure 7a,b). Although we have not calculated the van der Waals interactions in this study, it may be speculated that combined with the attractive van der Waals interaction, the modified electrostatic force might lead to a net attractive DLVO force between the particles when the cylinder potential is turned on. In other words, the presence of the charged confining wall might lead to a reduction in the repulsive energy barrier between the colloidal particles. In this manner, there might exist a possibility of a short-range DLVO attraction (or at least a substantial reduction in the repulsive interaction) that can induce particle aggregation. We however, emphasize that this attraction will not be solely due to electrostatic forces, which always remain repulsive. Furthermore, this overall DLVO attraction is manifested only at short interparticle separations and for large values of the parameter λ.

4.5. Interaction Force for Oppositely Charged Cylinder and Particles. The interaction forces were determined so far for situations where the particles and the cylinder surfaces had charges or potentials with same sign (like-charge cases). Figure 8 depicts the interaction force for cases where the cylinder surface is oppositely charged with respect to the particles. The figure depicts the interaction force on a sphere for $\kappa a = 1.0$, $\kappa h = 0.4$, and $\Psi_p = +3.0$. Figure 8a depicts the variation of the interaction force with λ for CP particles corresponding to different values of the cylinder surface potential. With increasing values of λ and the cylinder surface potential, the magnitude of the repulsive force increases. Comparing Figure 8a with Figure 5 indicates that while the net interaction force on the sphere increases for oppositely charged cylinder surfaces (Figure 8a), it

decreases for like-charged cylinder and particles (Figure 5). The results further indicate that the short-range repulsion between the particles can be dramatically amplified by trapping these in an oppositely charged cylindrical cavity.

The simulations of Figure 8b were performed under identical conditions as in Figure 8a, except for CC conditions on the particles. A similar increase of the interaction force between the spherical particles is observed when these are assigned CC boundary conditions for $0.1 < \lambda < 0.4$ (Figure 8b). At larger values of λ, however, the interaction force starts decreasing. For $\lambda > 0.8$, the interaction forces corresponding to different cylinder surface potentials are quite close ($20 < f_z < 30$), implying that for constant charge particles in a tightly fitting capillary, there will be very little influence of the capillary wall surface potential on the net interaction force on a particle.

These different behaviors of the interaction force for CP and CC particles in an oppositely charged capillary (specifically at large values of λ) might be helpful in distinguishing between different charging behaviors of the particles. For instance, from an inspection of the interaction forces between the particles as the cylinder wall is charged up, one might be able to conclude whether the particles are CP or CC, depending on whether the interaction force increases considerably or remains relatively unperturbed, respectively.

The short-range electrostatic interaction force between the particles was always repulsive as long as the particles were similarly charged (same surface potential or surface charge density), even when the cylindrical wall was oppositely charged. In fact, for CP particles, we observed an increase in the repulsive force when the sign of the cylinder surface potential was opposite to that of the particle surface potential.

The increase in the interaction force between two similarly charged spheres inside an oppositely charged cylindrical cavity can be explained by considering how the electric fields around the spheres are altered by the proximity of an oppositely charged surface. When an oppositely charged cylindrical wall approaches a spherical particle, the potential gradients around the sphere become larger (the surface charge density of the sphere increases). Hence, the two spheres will "see" each other as if they are becoming more charged as the cylinder wall approaches them. The increase is more prominent for constant potential particles (Figure 8a). The variation of the interaction force for constant charge particles originates from the distortion of the electric potential distribution around the particles in the presence of the oppositely charged cylinder wall. Although the charge densities of the particles remain fixed, the potential distribution around each sphere is altered by the presence of the cylinder, which in turn modifies the osmotic stress around the spheres. The variations of the osmotic stress cause the variation of the interaction force as the cylinder wall approaches the particles (Figure 8b).

To summarize, the interaction force between two spherical particles undergoes substantial modification in a confined cylindrical domain. The influence of the charged cylinder wall is most prominent when the cylinder radius is comparable to the particle radii. An interesting phenomenon observed in these simulations is that while like-charged cylinder surfaces tend to reduce the magnitude of the repulsion, oppositely charged walls considerably amplify the repulsion. Furthermore, the influence of the charged cylinder is more pronounced when the particles have constant potential surfaces.

5. Concluding Remarks

Solution of the nonlinear Poisson−Boltzmann equation to obtain the electrostatic interaction force between two spheres confined in a straight cylindrical capillary shows a large influence of the proximity of the charged cylinder wall on the net particle−particle interaction force. In developing the finite element based solution procedure, it has also been demonstrated that the short-range electrostatic interaction force between two spherical particles in an infinite domain can be evaluated accurately in a cylindrical coordinate system. Furthermore, we show that integration of the stress tensor over the surface of the particles yields a correct estimate of the interaction force.

The numerical solution of the nonlinear PB equation for two particles in a charged cylindrical cavity provides considerable insight regarding the influence of the cylinder wall on the interaction force between the particles. The interaction force between the particles under constant potential conditions diminishes when the cylinder wall is similarly charged. The short-range ($\kappa h < 1$) interaction force decreases from the corresponding particle−particle interaction force in an infinite medium by nearly an order of magnitude when the particles are enclosed in a similarly charged cylindrical cavity of comparable radius ($\lambda = a/b > 0.8$). Conversely, in an oppositely charged cylindrical capillary, the repulsive force between two constant potential particles increases considerably. Although the effects of the charged wall are not as pronounced for constant charge particles, there are still observable modifications of the short-range interaction force between the particles in the presence of the charged wall. From these simulations, it seems pertinent to explore the possibility of modulating the short-range electrostatic interaction force between constant potential particles by altering the surface potential of the confining cylindrical wall. Often, in such cases, nearly an order of magnitude modulation in the repulsive force between the particles may be obtained by changing the surface potential of the charged wall by a fraction of a volt.

Acknowledgment. The authors gratefully acknowledge financial support from the Natural Sciences and Engineering Research Council of Canada (NSERC) and the Alberta Ingenuity Fund toward this research. One of the authors (S.B.) also acknowledges financial support from the Canada Research Chairs Program.

Nomenclature

a	particle radius
b	pore radius
h	surface−surface separation distance between two spherical particles
e	electronic charge (1.6×10^{-19} C)
$\mathbf{E}$	electrostatic field vector
$\mathbf{F}$	force
f_z	scaled force acting along the z direction
F_z	component of force acting along the z direction
$\mathbf{I}$	identity tensor
k	Boltzmann constant (1.38×10^{-23} J K^{-1})
$\mathbf{k}$	unit vector in the positive z direction
$\mathbf{n}$	unit normal vector
n_∞	ionic number concentration in the bulk solution (m^{-3})
n_r, n_z	components of the unit normal along the r and z directions, respectively
q_p	surface charge density
Q_p	total surface charge

r	radial coordinate in the polar coordinate system
$\bar{r}$	scaled radial coordinate
T	absolute temperature
$\mathbf{T}_{ij}$	component of the stress tensor
z	axial coordinate in the polar coordinate system
$\bar{z}$	scaled axial coordinate

Greek Symbols

κ	inverse Debye screening length, eq 2
∇^2	Laplacian operator
$\partial\Omega$	boundary of the computational domain
ϵ_0	dielectric permittivity in a vacuum (8.8542×10^{-12} C^2 N^{-1} m^{-2})
ϵ	dielectric constant of the electrolyte
λ	dimensionless size ratio (a/b)
ν	absolute value of the valency for a (ν:ν) electrolyte solution
ψ	electrostatic potential
Ψ	scaled potential ($ve\psi/kT$)
Ψ_p, Ψ_c	dimensionless surface potentials of particle and cylinder, respectively
$\Psi_{p,\infty}$	surface potential of an isolated spherical particle
Ψ_r, Ψ_z	components of the electric field vector along the r and z directions, respectively
Π	osmotic pressure
σ_p	dimensionless surface charge density of a particle

Abbreviations

CC	constant charge
CP	constant potential
DLVO	Derjaguin−Landau−Verwey−Overbeek
EDL	electrostatic double layer
LW	Lifshitz−van der Waals
PB	Poisson−Boltzmann

LA0207567